Stochastic Modeling of Small-Scale, Anisotropic Structures in the Continental Upper Mantle

THOMAS H. JORDAN AND JAMES B. GAHERTY

Department of Earth, Atmospheric and Planetary Sciences
Massachusetts Institute of Technology, Cambridge, MA 02139

Abstract

New methods for the analysis of three-component seismograms have been applied to data from both continental and oceanic regions. Polarization anisotropy, manifested as the splitting of surface, guided, and shear body waves, has been observed in all regions, but no significant azimuthal anisotropy has been detected. This is expected if the local orientation of olivine crystals in the upper mantle is incoherent on the scale of the path lengths used in these experiments ($\Delta = 35°$–$50°$). From a detailed study of trans-Australia paths, we have shown that the shear-wave anisotropy in the western Australia craton averages 3-4% in the uppermost mantle, but it terminates abruptly at a Lehmann (L) discontinuity near a depth of 250 km. Our physical interpretation is that the L discontinuity beneath the ancient continental cratons marks the transition from an anisotropic mechanical boundary layer to a more isotropic region of a thick continental tectosphere. Above L, the temperatures have evidently remained cold enough to freeze-in the small-scale anisotropic structures and tectonic fabrics generated in episodes of orogenic compression associated with tectospheric stabilization. Below L, such structures were either never generated or were annealed out subsequent to their formation. These hypotheses about subcontinental structure have considerable bearing on a diverse set of geological and geodynamical problems, ranging from formation of the cratons to kimberlite vulcanism.

To provide additional quantitative tests of these hypotheses, we have formulated stochastic models that specify the small-scale heterogeneity of the continental upper mantle as samples of Gaussian random fields with self-affine (fractal) scaling at high wavenumbers. We approximate the spatial variations in elasticity $C(\mathbf{x})$ as a hexagonal tensor field with a local axis of symmetry given by a unit vector field $\hat{\mathbf{s}}(\mathbf{x})$. We impose the structure of a stationary Gaussian random field on $\mathbf{s}(\mathbf{x})$ and, from a deterministic functional relationship between C and s, calculate the ensemble averages of $C(\mathbf{x})$ that are needed to describe low-frequency wave propagation. Solving forward problems of this type allows us to set up quantitative inverse problems for the parameters of the stochastic distributions. In the modeling discussed here, s is assumed to have transversely isotropic stochastic symmetry and to be specified by four statistical parameters: an aspect ratio of the anisotropy, ξ, a characteristic horizontal wavenumber of the heterogeneity, k, an aspect ratio of the heterogeneity, η, and a fractal dimension, D. For $\xi = 1$, the distribution of $\hat{\mathbf{s}}$ is isotropic in all three directions; in the limit $\xi \to \infty$, s_3 equals zero with probability one, and $\hat{\mathbf{s}}$ is isotropically distributed in the horizontal plane. We show that the upper-mantle anisotropy in Gaherty and Jordan's [1995] model AU3 is consistent with Voigt averages given by $\xi \approx 2$-3. We discuss how better approximations to the effective elastic tensor can be obtained from a self-consistent, second-order Born approximation.

Objectives

The technologies of nuclear-monitoring seismology are built, in part, on studies of wave propagation at regional distances (< 2000 km). One poorly understood aspect of regional propagation is the forward scattering of high-frequency signals by small inhomogeneities. The objectives of this research are threefold: (1) to formulate parameterized stochastic models of small-scale heterogeneity that are suitable for assessing scattering effects at regional distances, (2) to constrain the model parameters using broadband seismic data, and (3) to assess the implications of these models for regional wave propagation related to nuclear monitoring.

Research Accomplishments: Observations and Modeling of Seismic Corridors

Our approach is to model small-scale heterogeneity by a bootstrap from low to high frequencies [Jordan and Gaherty, 1994]. In the first phase of this program, we have used low-frequency (< .05 Hz), phase-coherent waves to derive anisotropic, path-averaged models of crustal and upper-mantle structure. We have developed methods for extracting phase delays and amplitudes from three-component seismograms that have delivered new information about impedance discontinuities and velocity gradients in the upper mantle [Revenaugh and Jordan, 1991; Gee and Jordan, 1992], and we have applied them to data from both continental [Gaherty and Jordan, 1995] and oceanic [Gaherty et al., 1995] regions. Polarization anisotropy, manifested as the splitting of surface, guided, and shear body waves, has been observed in all regions, but no significant azimuthal anisotropy has been detected. This is expected if the local orientation of olivine crystals in the upper mantle is incoherent on the scale of the path lengths used in these studies ($\Delta = 35°–50°$). We have therefore modeled the splitting in terms of radially anisotropic, but transversely isotropic, elasticity. From a detailed study of trans-Australia paths [Gaherty and Jordan, 1995], we have shown that the shear-wave anisotropy in the western Australia craton averages 3-4% in the uppermost mantle, but it terminates abruptly at a Lehmann (L) discontinuity near a depth of 250 km. At the L transition, which occurs over a depth range of less than 30 km, the average SV wavespeed increases and the average SH wavespeed decreases, obtaining nearly equal values in the mantle layer between L and the 410-km discontinuity.

Our physical interpretation is that the L discontinuity beneath the ancient continental cratons marks the transition from an anisotropic mechanical boundary layer to a more isotropic region of a thick continental tectosphere [Revenaugh and Jordan, 1991; Gaherty and Jordan, 1995]. Above L, the temperatures have evidently remained cold enough to freeze-in the small-scale anisotropic structures and tectonic fabrics generated in episodes of orogenic compression associated with tectospheric stabilization [Jordan, 1988; Silver and Chan, 1991]. Below L, such structures were either never generated, perhaps because L coincides with a transition from dislocation to diffusion creep [Karato, 1992], or were annealed out subsequent to their formation. These hypotheses about subcontinental structure have considerable bearing on a diverse set of geological and geodynamical problems, ranging from formation of the cratons to kimberlite vulcanism [Gaherty and Jordan, 1995].

Research Accomplishments: Stochastic Modeling of Fine-Scale Anisotropic Structures

In the current phase of our research program, we are focusing on the interpretation of polarization anisotropy in terms of heterogeneity at subwavelength scales. We have formulated stochastic models that specify the small-scale heterogeneity of the continental upper mantle as samples of Gaussian random fields with self-affine (fractal) scaling at high wavenumbers, and we have derived expressions relating the parameters of these models to the speeds of low-frequency seismic waves. This report presents some of these results and outlines future research activity related to this modeling.

We consider a medium governed by a linear stress-strain relation $\sigma_{ij} = C_{ijkl}\varepsilon_{kl}$, where the elasticity tensor $\mathbf{C}$ has Cartesian components $\{C_{ijkl}(\mathbf{x}): i,j,k,l = 1,2,3\}$ that are functions of three-dimensional position vector $\mathbf{x}$. Theoretical calculations [Estey and Douglas, 1986] and measurements on kimberlite xenoliths [Mainprice and Silver, 1993; Christensen, 1994] indicate that the elasticity of upper-mantle peridotites has quasi-hexagonal symmetry on the hand-sample scale. Therefore, it is reasonable to approximate $\mathbf{C}(\mathbf{x})$ as a hexagonal tensor field with a local axis of symmetry given by the unit vector $\hat{\mathbf{s}}(\mathbf{x}) = \mathbf{s}(\mathbf{x})/|\mathbf{s}(\mathbf{x})|$. This can be accomplished by restricting the tensor field to be a functional of a vector field $\mathbf{s}(\mathbf{x})$: $\mathbf{C}(\mathbf{x}) = \mathbf{C}(\mathbf{s}(\mathbf{x}))$. In petrological terms, $\hat{\mathbf{s}}(\mathbf{x})$ is largely determined by the local average orientation of the a axis of olivine, which is aligned by mantle deformation [Estey and Douglas, 1986]. Our strategy is to impose the structure of a Gaussian random field on $\mathbf{s}(\mathbf{x})$ and, from the functional relationship $\mathbf{C}(\mathbf{s})$, to calculate the ensemble averages of $\mathbf{C}(\mathbf{x})$ that are needed to describe low-frequency wave propagation. Solving this forward problem will allow us to assess the applicability of the stochastic models to the continental upper mantle and, if justified, to set up quantitative inverse problems for the parameters of the stochastic distributions.

Specification of the Vector Field. Within some region of the upper mantle, the Gaussian random field $\mathbf{s}(\mathbf{x})$ is assumed to be stationary with zero mean, $\langle \mathbf{s}(\mathbf{x}) \rangle = 0$, and thus specified by its autocovariance matrix, $C_{ss}(\mathbf{x}) = \langle \mathbf{s}(\mathbf{x}')\mathbf{s}^T(\mathbf{x}'+\mathbf{x}) \rangle$. C_{ss} is symmetric and positive definite and admits the zero-lag eigenvector expansion

$$C_{ss}(0) \equiv \mathbf{S}_0^2 = \sum_{n=1}^{3} \sigma_n^2 \hat{\mathbf{e}}_n \hat{\mathbf{e}}_n^T . \tag{1}$$

We specialize this matrix in the following way: its last eigenvector is assumed to be vertical, $\hat{\mathbf{e}}_3 = \hat{\mathbf{z}}$, with dimensionless variance ξ^2, and the variances of the other two eigenvectors are set equal to unity. Hence, the s field is required to be statistically isotropic in the xy plane, with principal components having root-mean-square (r.m.s.) variations given by

$$\sigma_1 = \sigma_2 = \xi\,\sigma_3 = 1. \tag{2}$$

We will call the dimensionless parameter ξ the *aspect ratio of the anisotropy*. In terms of the coordinates $s_1 = s\sin\theta\cos\varphi$, $s_2 = s\sin\theta\sin\varphi$, $s_3 = s\cos\theta$, the three-dimensional probability density element (p.d.e.) for s can be written

$$p(\mathbf{s})dV(\mathbf{s}) = \frac{\xi}{(2\pi)^{3/2}}e^{-\frac{1}{2}(s_1^2+s_2^2+\xi^2 s_3^2)}\,ds_1\,ds_2\,ds_3$$

$$= \frac{\xi}{(2\pi)^{3/2}}e^{-s^2/2}e^{\kappa(s)\cos^2\theta}s^2\,ds\sin\theta\,d\theta\,d\varphi, \qquad \kappa(s) \equiv \frac{1}{2}s^2(1-\xi^2). \qquad (3)$$

From this expression, it can be seen that the p.d.f. on a sphere of radius s corresponds to a Watson distribution with dispersion parameter $\kappa(s)$ [Fisher et al., 1987]. For $\xi = 1$, the distribution of $\hat{\mathbf{s}}$ is isotropic in all three directions. Where $\xi < 1$, the probability of $\hat{\mathbf{s}}$ is concentrated towards the vertical axis (bipolar distribution, $\kappa > 0$); where $\xi > 1$, it is concentrated towards the equatorial plane (girdle distribution, $\kappa < 0$). In the limit $\xi \to \infty$, s_3 equals zero with probability one, and $\hat{\mathbf{s}}$ is isotropically distributed in the xy plane. For fixed ξ, the conditional distribution $p(\hat{\mathbf{s}} \mid s)$ becomes more isotropic as $s \to 0$.

To specify the spatial correlation of the $\mathbf{s}$ field, we define the Riemannian length,

$$r^2(\mathbf{x}) = \mathbf{x}^T\mathbf{Q}\,\mathbf{x}, \qquad (4)$$

$\mathbf{Q}$ is a symmetric positive-definite matrix chosen, like $\mathbf{S}_0$, to be transversely isotropic; i.e., to have eigenvectors $\{\hat{\mathbf{e}}_1, \hat{\mathbf{e}}_2, \hat{\mathbf{e}}_3 = \hat{\mathbf{z}}\}$ and eigenvalues

$$k_1^2 = k_2^2 = \eta^2 k_3^2 \equiv k^2. \qquad (5)$$

We adopt an autocovariance matrix of the form

$$C_{\mathbf{ss}}(\mathbf{x}) = \mathbf{S}_0^2\,\rho(r(\mathbf{x})), \qquad (6)$$

where $\rho(r)$ is a scalar-valued autocorrelation function such that $\rho(0) = 1$ and $\lim_{r\to\infty}\rho(r) = 0$. A convenient and useful function with these properties is

$$\rho(r) = 2^{-(\nu+1)}r^\nu K_\nu(r)/\Gamma(\nu), \qquad 0 \le r < \infty, \ 0 \le \nu < 1 \qquad (7)$$

Here $K_\nu(r)$ is the modified Bessel function of the second kind and $\Gamma(\nu)$ is the gamma function. This anisotropic autocorrelation function was introduced as a stochastic representation of seafloor roughness by Goff and Jordan [1988], who describe many of its properties. A three-dimensional Fourier transform yields the power spectrum:

$$P(\mathbf{k}) = \int\rho(r(\mathbf{x}))e^{-i\mathbf{k}^T\mathbf{x}}\,dV(\mathbf{x}) = 8\pi^{3/2}\frac{\Gamma(\nu+3/2)}{\Gamma(\nu)}|\mathbf{Q}|^{-1/2}[\mathbf{k}^T\mathbf{Q}^{-1}\mathbf{k} + 1]^{-(\nu+3/2)} \qquad (8)$$

This spectral density has principal axes $\hat{\mathbf{e}}_1, \hat{\mathbf{e}}_2, \hat{\mathbf{e}}_3$ with corner wavenumbers $k, k, \eta k$; it is flat below these corners and rolls off above them at an asymptotic rate of $-(2\nu + 3)$. Realizations of this Gaussian field are thus characterized by two outer scales: k^{-1} in the xy plane, and $(\eta k)^{-1}$ in the z direction. The dimensionless parameter η is termed the *aspect ratio of the heterogeneity*. At scales much smaller than $(\eta k)^{-1}$, the field is statistically self-affine with scaling parameter ν, and it has a Hausdorff (fractal) dimension of

$$D = 4 - \nu \qquad (9)$$

(see the appendix of Goff and Jordan [1988] for definitions and proofs). The special case $v = 1/2$ corresponds to the exponential correlation function, $\rho(r) = e^{-r}$, that has been commonly used in theoretical studies of wave scattering [e.g., Chernov, 1960].

In summary, we have constructed a dimensionless vector field s that has a transversely isotropic stochastic symmetry. Its statistics are described by a single dimensionalized parameter, the characteristic horizontal wavenumber of the heterogeneity k, $([k] = length^{-1})$, and three dimensionless numbers: the aspect ratio of the anisotropy ξ, the aspect ratio of the heterogeneity η, and the fractal dimension D. Figures 1 and 2 illustrate sections taken through some realizations of this Gaussian random field for $k^{-1} = 200$ km, D = 3.2, and several values of ξ and η.
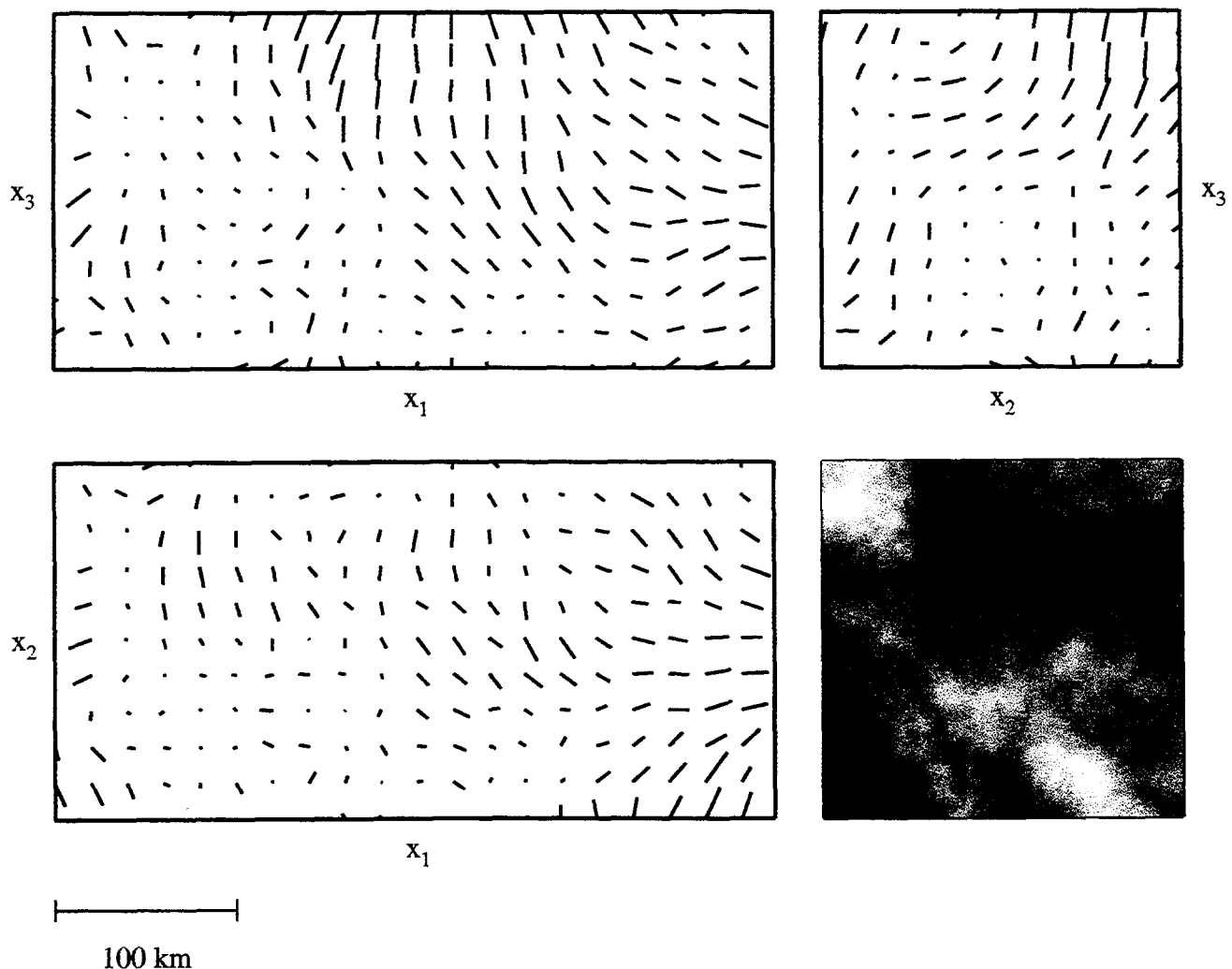

x_3 x_1

x_3 x_2

x_2 x_1

100 km

Figure 1. A realization of the vector field s for $k^{-1} = 200$ km, D = 3.2, and $\xi = \eta = 1$. The vectors are calculated on a 20 km × 20 km grid and displayed as their projections onto the sides of a 500 km × 200 km × 200 km rectangular domain. Lower right panel is a grayshade plot of the x_2 coordinate of s in the x_2-x_3 plane, showing the structure of the field at higher resolution than the vector sampling. In this case, the field is statistically isotropic in all directions in both the vector orientation and the heterogeneity.
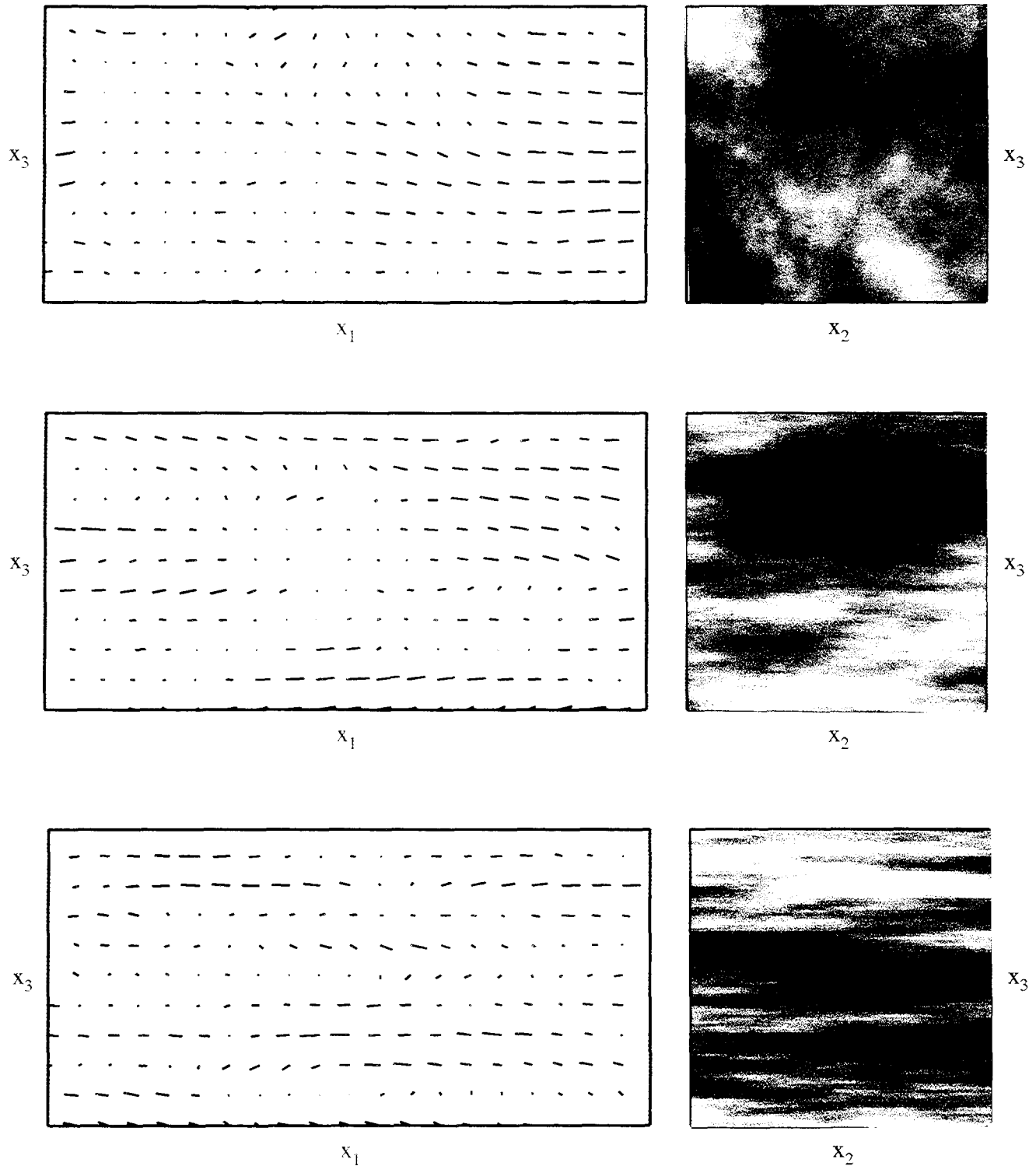
437

Figure 2. Realizations of the vector field **s** for $k^{-1} = 200$ km, $D = 3.2$, and $\xi = 5$, and values of the heterogeneity aspect ratio η equal to 1 (*top*), 5 (*middle*), and 10 (*lower*). In each case, the left and right panels are plotted with the same conventions as the upper-left and lower-right panels of Figure 1, respectively. The field in the top panel has statistically isotropic heterogeneity but anisotropic vector orientation. The field in the lower panel corresponds to an anisotropic stochastic laminate ($\eta \gg 1$). All realizations are isotropic in the x_1-x_2 plane.

438

Representation of the Elasticity Field. The Gaussian random field structure of $s(\mathbf{x})$ is mapped onto the elasticity tensor field $\mathbf{C}(\mathbf{x})$ through a deterministic functional relationship $\mathbf{C}(s)$. If $\mathbf{C}$ is a functional of s, then it must be hexagonal with symmetry axis $\hat{s}$. Any hexagonally symmetric elasticity tensor with components C_{ijkl} can be represented by six elastic parameters, which are taken here to be

$$C_{1111} = c_{11} = a, \qquad C_{1122} = c_{12} = b, \qquad C_{3333} = c_{33} = c,$$

$$C_{1133} = c_{13} = f, \qquad C_{1212} = c_{44} = m, \qquad C_{1313} = c_{55} = l. \tag{10}$$

Only five of these parameters are independent, because the symmetry requires

$$b = a - 2m. \tag{11}$$

An alternative and analytically convenient representation is the Backus [1970] harmonic decomposition:

$$C_{ijkl} = \mathfrak{D}^{(4)}_{ijkl} H^{(4)} + \mathfrak{D}^{(2)}_{ijkl} H^{(2)} + \mathfrak{D}^{(0)}_{ijkl} H^{(0)} + d^{(2)}_{ijkl} h^{(2)} + d^{(0)}_{ijkl} h^{(0)}. \tag{12}$$

Here $H^{(\ell)}$ and $h^{(\ell)}$ are harmonic polynomials of degree ℓ, and $\mathfrak{D}^{(\ell)}_{ijkl}$ and $d^{(\ell)}_{ijkl}$ are the ℓth-order differential operators (δ_{ij} is the Kronecker delta),

$$\mathfrak{D}^{(4)}_{ijkl} = \frac{1}{4!} \partial_i \partial_j \partial_k \partial_l, \tag{13a}$$

$$\mathfrak{D}^{(2)}_{ijkl} = \frac{1}{2!}(\delta_{ij}\partial_k \partial_l + \delta_{kl}\partial_i \partial_j + \delta_{ik}\partial_j \partial_l + \delta_{jl}\partial_i \partial_k + \delta_{il}\partial_j \partial_k + \delta_{jk}\partial_i \partial_l), \tag{13b}$$

$$\mathfrak{D}^{(0)}_{ijkl} = \delta_{ij}\delta_{kl} + \delta_{ik}\delta_{jl} + \delta_{il}\delta_{jk}, \tag{13c}$$

$$d^{(2)}_{ijkl} = \frac{1}{2!}(\delta_{ij}\partial_k \partial_l + \delta_{kl}\partial_i \partial_j - \frac{1}{2}\delta_{ik}\partial_j \partial_l - \frac{1}{2}\delta_{jl}\partial_i \partial_k - \frac{1}{2}\delta_{il}\partial_j \partial_k - \frac{1}{2}\delta_{jk}\partial_i \partial_l), \tag{13d}$$

$$d^{(0)}_{ijkl} = \delta_{ij}\delta_{kl} - \frac{1}{2}\delta_{ik}\delta_{jl} - \frac{1}{2}\delta_{il}\delta_{jk}. \tag{13e}$$

For a hexagonal fourth-order tensor with symmetry axis $\hat{s}$, the harmonic polynomials are

$$H^{(4)}(\mathbf{r}) = 8 H_4 r^4 P_4(\hat{s}^T \hat{r}), \tag{14a}$$

$$H^{(2)}(\mathbf{r}) = -2 H_2 r^2 P_2(\hat{s}^T \hat{r}), \tag{14b}$$

$$H^{(0)}(\mathbf{r}) = H_0, \tag{14c}$$

$$h^{(2)}(\mathbf{r}) = -2 h_2 r^2 P_2(\hat{s}^T \hat{r}), \tag{14d}$$

$$h^{(0)}(\mathbf{r}) = h_0, \tag{14e}$$

where $P_\ell(\cos\Delta)$ is the Legendre polynomial of order ℓ and $\Delta = \text{acos}(\hat{\mathbf{s}}^T \hat{\mathbf{r}})$ is the angle between $\mathbf{r}$ and $\mathbf{s}$. As shown by Backus [1970], the three polynomials $\{ H^{(\ell)} : \ell = 0,2,4 \}$ represent the totally symmetric part of $\mathbf{C}$, whereas the two polynomials $\{ h^{(\ell)} : \ell = 0,2 \}$ represent its antisymmetric part. The elastic constants in (10) are related to the coefficients H_ℓ and h_ℓ by

$$a = 3H_4 + 6H_2 + 3H_0, \tag{15a}$$

$$b = H_4 + 2H_2 + H_0 + 2h_2 + h_0, \tag{15b}$$

$$c = 8H_4 - 12H_2 + 3H_0, \tag{15c}$$

$$f = -4H_4 - H_2 + H_0 - h_2 + h_0, \tag{15d}$$

$$l = -4H_4 - H_2 + H_0 + \frac{1}{2}h_2 - \frac{1}{2}h_0, \tag{15e}$$

$$m = H_4 + 2H_2 + H_0 - h_2 - \frac{1}{2}h_0. \tag{15f}$$

(Here we have corrected some errors in equation (34) of Backus [1970].)

To complete the functional relationship between $\mathbf{C}$ and $\mathbf{s}$, we specify the elastic parameters to be monomials in the vector length s:

$$H_\ell(\mathbf{s}) = \hat{H}_\ell s^n, \quad h_\ell(\mathbf{s}) = \hat{h}_\ell s^n, \tag{16}$$

where n is a non-negative integer that is constant for all ℓ. We call this additional model parameter *the strength exponent*. In the case $n = 0$, the harmonic coefficients are independent of position, and $C_{ijkl}(\mathbf{x})$ is a constant tensor rotated to have an axis of symmetry $\hat{\mathbf{s}}(\mathbf{x})$.

<u>Voigt Average</u>. The Voigt average is the expected value of the elasticity tensor, $\overline{C}_{ijkl} = \langle C_{ijkl}(\mathbf{x}) \rangle$, which can be calculated directly from the expected values of the harmonic polynomials. The latter can be expressed as sums over the integrals

$$\int s^n P_\ell(\cos\Delta(\hat{\mathbf{s}})) p(\mathbf{s}) dV(\mathbf{s}). \tag{17}$$

Integrating the Legendre polynomials term-by-term yields

$$\overline{H}^{(4)}(\mathbf{r}) = \hat{H}_4 (35 I_4^n - 30 I_2^n + 3 I_0^n) r^4 P_4(\hat{\mathbf{z}}^T \hat{\mathbf{r}}), \tag{18a}$$

$$\overline{H}^{(2)}(\mathbf{r}) = -\hat{H}_2 (3 I_2^n - I_0^n) r^2 P_2(\hat{\mathbf{z}}^T \hat{\mathbf{r}}), \tag{18b}$$

$$\overline{H}^{(0)}(\mathbf{r}) = \hat{H}_0 I_0^n, \tag{18c}$$

$$\overline{h}^{(2)}(\mathbf{r}) = -\hat{h}_2 (3 I_2^n - I_0^n) r^2 P_2(\hat{\mathbf{z}}^T \hat{\mathbf{r}}), \tag{18d}$$

$$h^{(0)}(\mathbf{r}) = h_0.$$ (18e)

Hence, the Voigt average is transversely isotropic with a vertical symmetry axis, as expected for a random medium whose statistics have this symmetry. The integrals appearing in (18) are

$$I_\ell^n(\xi) = \int_0^1 \frac{\xi\, x^\ell}{[1 + (\xi^2 - 1)x^2]^{(n+3)/2}}\, dx$$ (19)

We give explicit forms for $n = 0, 1$:

$$I_0^0 = 1,$$ (20a)

$$I_2^0 = \frac{1}{\xi^2 - 1}\left(\frac{\xi}{\sqrt{\xi^2 - 1}} \operatorname{asinh}\sqrt{\xi^2 - 1} - 1 \right),$$ (20b)

$$I_4^0 = \frac{1}{2(\xi^2 - 1)}\left(1 - 3 I_2^0\right),$$ (20c)

$$I_0^1 = \frac{\xi}{\sqrt{\xi^2 - 1}} \operatorname{atan}\sqrt{\xi^2 - 1},$$ (21a)

$$I_2^1 = \frac{1}{\xi^2 - 1}\left(I_0^1 - \frac{1}{3} \right),$$ (21b)

$$I_4^1 = \frac{1}{\xi^2 - 1}\left(\frac{1}{\xi} - 3 I_2^1 \right).$$ (21c)

Application to the Upper Mantle. We have applied this theory to the interpretion of the anisotropy observed by Gaherty and Jordan [1995]. Their model AU3 has a radially anisotropic region extending from the M discontinuity at 30 km depth to the L discontinuity at 252 km depth. The magnitude of the anisotropy in such a transversely isotropic model is measured by an S-wave anisotropy ratio, $(v_{SH} - v_{SV}) / v_{SV}$, and a similar ratio for P wavespeeds. At the base of the AU3 anisotropic region, these ratios are both about 4%. In comparison, the anisotropy ratios calculated for a pyrolite mineralogy in which the olivine and pyroxene crystals have been completely aligned by shear deformation in the horizontal plane (but randomly oriented within that plane) is about 7% [Estey and Douglas, 1986]. Within the context of our stochastic model, this type of average corresponds to $\xi = \infty$, describing the (geologically unexpected) situation where all the s vectors are horizontal. As ξ decreases, the anisotropy ratios decrease, achieving values comparable to AU3 for $\xi \approx 2\text{-}3$. Figure 3 shows this behavior for the Voigt average in the case where $n = 0$. An anisotropy aspect ratio of this magnitude is geologically reasonable, although it must be admitted that not much is known from direct observation about what ξ should be. The results in Figure 3 at least suggests that our approach to the stochastic modeling of fine-scale upper-mantle structure might be on the right track.
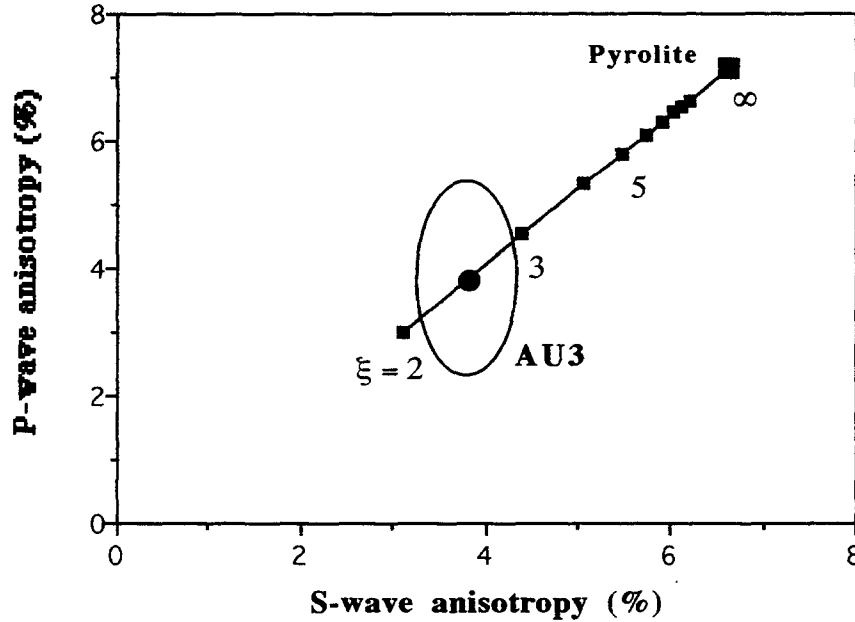
Figure 3. Plot of the P-wave anisotropy, $(v_{PH} - v_{PV}) / v_{PV}$, versus the S-wave anisotropy, $(v_{SH} - v_{SV}) / v_{SV}$. The point with the 1-$\sigma$ error ellipse is the upper-mantle value from model AU3 of Gaherty and Jordan [1995]. The large square is the value calculated by Voigt averaging the hexagonally symmetric pyrolite model of Estey and Douglas [1986] assuming complete crystallographic alignment in the horizontal plane ($\xi = \infty$). The small squares are Voigt averages for a strength exponent $n = 0$ at integer values of the anisotropy aspect ratio ξ, showing how the apparent anisotropy decreases as the local orientation becomes statistically more isotropic. This calculation suggests that the value of ξ appropriate for the Australian upper mantle is on the order of 2 or 3.

Our analysis is not complete, however. The one-point probability density $p(s)$ is independent of the two-point correlation parameters; hence, the Voigt average depends only on the aspect ratio of the anisotropy ξ and the strength exponent n. On the other hand, the effective anisotropy sensed by low-frequency waves must also be dependent on the aspect ratio of the heterogeneity η. This illustrates the well known fact that the Voigt average can be a poor approximation to the effective elasticity tensor governing low-frequency wave propagation [Backus, 1962; Berryman, 1994].

Self-Consistent Effective Media Theory: The Second-Order Born Approximation. Better approximations can be obtained from self-consistent theories of effective media based on an integral-equation formulation of the scattering problem. This technique was developed and first applied to polycrystalline aggregates by Korringa[1973], and Zeller and Dederichs [1973]; see reviews by Gubernatis and Krumhansl [1975], Domany et al. [1975], and Berryman [1994]. In the long-wavelength limit, the time derivatives of the dynamic displacement field commute with ensemble averaging, so that the effective elasticity tensor

$$\tilde{C}_{ijkl} = \langle \sigma_{ij} \rangle \langle \varepsilon_{kl} \rangle^{-1} \tag{22}$$

can be calculated from the static problem. The development of these theories begins by expressing $C_{ijkl}(\mathbf{x})$ as the sum of a constant tensor C^0_{ijkl} and a perturbation $\delta C_{ijkl}(\mathbf{x})$; then, the condition for static equilibrium can be put in the form of a Lippman-Schwinger equation

$$\varepsilon_{ij}(\mathbf{x}) = \varepsilon^0_{ij}(\mathbf{x}) + \int G_{ijkl}(\mathbf{x},\mathbf{x}')\delta C_{klmn}(\mathbf{x}')\varepsilon_{mn}(\mathbf{x}')dV(\mathbf{x}'). \tag{23}$$

G_{ijkl} is the strain Green's function corresponding to $C_{ijkl}(\mathbf{x})$. In operator notation, this equation can be written as $\varepsilon = \varepsilon^0 + \mathbf{G}\,\delta\mathbf{C}\,\varepsilon$ and solved iteratively via a Born series. The series can be summed to obtain

$$\varepsilon = \varepsilon^0 + \mathbf{G}\mathbf{T}\varepsilon^0, \tag{24}$$

$$\mathbf{T} \equiv \delta\mathbf{C}(\mathbf{I} - \mathbf{G}\,\delta\mathbf{C})^{-1} = \delta\mathbf{C} + \delta\mathbf{C}\mathbf{G}\,\delta\mathbf{C} + \delta\mathbf{C}\mathbf{G}\,\delta\mathbf{C}\mathbf{G}\,\delta\mathbf{C} + \cdots. \tag{25}$$

The fourth-order tensor defined in (25) is equivalent to the T matrix of quantum mechanics, and the nth-order term in its series (Born) expansion expresses the scattering process of order $n - 1$. Using (24) in (22) yields the exact solution

$$\tilde{\mathbf{C}} = \mathbf{C}^0 + (\mathbf{I} - \langle\mathbf{G}\mathbf{T}\rangle)^{-1}\langle\mathbf{T}\rangle. \tag{26}$$

Because the exact evaluation of the second term in (26) is infeasible (e.g., $\mathbf{G}$ must be calculated for $\mathbf{C}(\mathbf{x})$), we resort to a self-consistent approximation: $\mathbf{C}^0$, which has thus far been arbitrary, is chosen to equal $\tilde{\mathbf{C}}$, so that (26) is recovered if $\langle\tilde{\mathbf{T}}\rangle = 0$. Substituting the Born expansion in (25) generates a sum in which the nth term is a contraction of the $(n-1)$th outer product of $\tilde{\mathbf{G}}$ against the n-point moment of $\delta\mathbf{C}$.

Truncating the Born series at first order yields the Voigt average, $\tilde{\mathbf{C}} \approx \overline{\mathbf{C}}$. To obtain a better approximation, we have carried the expansion to second order. Since $\tilde{\mathbf{C}} - \overline{\mathbf{C}} \sim O(\delta\mathbf{C})$, the second-order Born approximation takes the form of an implicit integral equation,

$$\tilde{C}_{ijkl} \approx \overline{C}_{ijkl} + \int \tilde{G}_{pqrs}(\mathbf{x})\mathcal{V}_{ijpqrskl}(\mathbf{x})dV(\mathbf{x}), \tag{27}$$

where $\tilde{G}_{pqrs}$ is the strain Green's function for a transversely isotropic medium with a constant elasticity tensor $\tilde{C}_{ijkl}$, and $\mathcal{V}_{ijklpqrs}$ are the components of the eighth-order, spatially stationary covariance tensor $\mathcal{V}(\mathbf{x}) \equiv C_{\mathbf{CC}}(\mathbf{x})$,

$$\mathcal{V}_{ijklpqrs}(\mathbf{x}) = \langle[C_{ijkl}(\mathbf{x}') - \overline{C}_{ijkl}][C_{pqrs}(\mathbf{x}'+\mathbf{x}) - \overline{C}_{pqrs}]\rangle. \tag{28}$$

$\mathcal{V}(\mathbf{x})$ can be evaluated from the Backus harmonic decomposition (12) by integrating two-point products of the harmonic polynomials against the joint p.d.f. $p(\mathbf{s}',\mathbf{s}'+\mathbf{s})$. This allows us to fully exploit the transversely isotropic stochastic symmetry of the C field. Moreover, we can obtain considerable simplifications by rewriting the second term in (27) as an integral over the wavevector $\mathbf{k}$; e.g., the 3D Fourier transform of $\tilde{G}(\mathbf{x})$ depends only on $\hat{\mathbf{k}}$, and the spatial derivatives in (12) reduce to multiplications by k_i. We are currently developing an iterative method for calculating (27) using this approach.

References

Backus, G. E., Long-wave elastic anisotropy produced by horizontal layering, *J. Geophys. Res.*, *67*, 4427-4440, 1962.

Backus, G. E., A geometrical picture of anisotropic elastic tensors, *Rev. Geophys. Space Phys.*, *8*, 633-671, 1970.

Berryman, J. G., Mixture theories for rock properties, in *Rock Physics and Phase Relations*, AGU Reference Shelf #3, American Geophysical Union, Washington, D.C., 1994.

Chernov, L. A., *Wave Propagation in a Random Medium*, McGraw-Hill, New York, 1960.

Christensen, N. I., Seismic properties of mantle xenoliths: clues to the interpretation of deep seismic observations beneath the kimberlite province of Yakutsia, unpublished manuscript, January, 1994.

Domany, E., J. E. Gubernatis, and J. A. Krumhansl, The elasticity of polycrystals and rocks, *J. Geophys. Res.*, *80*, 4851-4856, 1975.

Estey, L. H., and B. J. Douglas, Upper-mantle anisotropy: a preliminary model, *J. Geophys. Res.*, *91*, 11393-11406, 1986.

Fisher, N. I., T. Lewis, and B. J. J. Embleton, *Statistical Analysis of Spherical Data*, Cambridge University Press, Cambridge, 329 pp., 1987.

Gaherty, J. B., and T. H. Jordan, Lehmann discontinuity as the base of an anisotropic layer beneath continents, *Science*, *268*, 1468-1471, 1995.

Gaherty, J. B., T. H. Jordan, and L. S. Gee, Seismic structure of the upper mantle in a western Pacific corridor, *J. Geophys. Res.*, submitted, August, 1995.

Gee, L. S., and T. H. Jordan, Polarization anisotropy and fine-scale structure of the Eurasian upper mantle, *Geophys. Res. Lett.*, *15*, 824-827, 1988.

Gee, L. S., and T. H. Jordan, Generalized seismological data functionals, *Geophys. J. Int.*, *111*, 363-390, 1992.

Goff, J., and T. H. Jordan, Stochastic modeling of seafloor morphology: inversion of Sea Beam data for second-order statistics, *J. Geophys. Res.*, *93*, 13589-13608, 1988.

Gubernatis, J. E., and J. A. Krumhansl, Macroscopic engineering properties of polycrystalline materials: elastic properties, *J. Appl. Phys.*, *46*, 1875-1883, 1975.

Karato, S., On the Lehmann discontinuity, *Geophys. Res. Lett.*, *19*, 2255-2258, 1992.

Korringa, J., Theory of eslastic constants of heterogeneous media, *J. Math. Phys.*, *14*, 509-513, 1973.

Jordan, T. H., Structure and formation of the continental tectosphere, *J. Petrology Special Lithosphere Issue*, 11-37, 1988.

Jordan, T. H., and J. B. Gaherty, Polarization anisotropy and small-scale structure of the continental upper mantle, *Proceedings of the 16th Annual Seismic Research Symposium*, PL-TR-94-2217, Phillips Laboratory, Massachusetts, pp. 189-195, 1994. ADA284667

Mainprice, D., and P. Silver, *Phys. Earth Planet. Inter.*, *78*, 257, 1993.

Revenaugh, J.R. and T.H. Jordan, Mantle layering from *ScS* reverberations, 3, The upper mantle, *J. Geophys. Res.*, *96*, 19,781-19,810, 1991.

Silver, P.G. and W.W. Chan, Shear-wave splitting and subcontinental mantle deformation, *J. Geophys. Res.*, *96*, 16,429-16,454, 1991.

Zeller, R., and P. H. Dederichs, Elastic constants of polycrystals, *Phys. Status Solidi (b)*, *55*, 831-842, 1973.